JACS
JOURNAL OF THE AMERICAN CHEMICAL SOCIETY
pubs.acs.org/JACS
Article

Nature-Inspired Glycosylation Strategy Enabled Hydrosoluble Polyhydric Thioalkylated Ferrocene Derivatives for pH-Neutral Aqueous Redox Flow Batteries

Guochun Ding, Tianyu Shen, Pengbo Zhang, Zuoao Wu, Qianchuan Yu, Yuzhu Liu, Sheng Wen, Jie Wei, Zuoxiu Tie,* Yichao Yan,* and Zhong Jin*

Cite This: https://doi.org/10.1021/jacs.5c11833

ABSTRACT: Organic molecules have been regarded as promising alternatives in aqueous redox flow batteries, with the aim of reducing reliance on mineral resources. Enhancing the solubility and stability of organic species is essential and requires strategic functional group refinement and molecular structure optimization. However, there are relatively few solubilization strategies of naturally water-solubilizing groups in ARFBs. Sugars, i.e., carbohydrates, ubiquitous in nature and indispensable as nutrients, possess an exceptional hydrophilic property and offer a sustainable pathway for molecular functionalization. Herein, we present a thioglucose functionalization strategy to synthesize highly soluble ferrocene derivatives via convenient thioetherification reactions under mild conditions. Under the hydrophilic effect of abundant highly polar hydroxyl moieties, the as-synthesized glycosyl-functionalized thioalkylated ferrocene derivative, namely, Fc-(Thio-Glc)$_2$, exhibits high water solubility (1.3 M in 1.0 M KCl solution) and favorable electrochemical properties. Molecular dynamics simulations manifest the effects of hydrogen bond networks on the molecular configuration and solvation behavior. Ex situ spectroscopic analyses confirmed the high reversibility and long-term operation stability of Fc(Thio-Glc)$_2$. Consequently, the pH-neutral ARFBs assembled with the 0.5 M Fc(Thio-Glc)$_2$ catholyte achieve a capacity retention of 99.995% per cycle or 99.82% per day. This study highlights the tremendous potential of a bioinspired molecular engineering strategy in advancing safe, stable, and sustainable ARFBs toward large-scale energy storage applications.

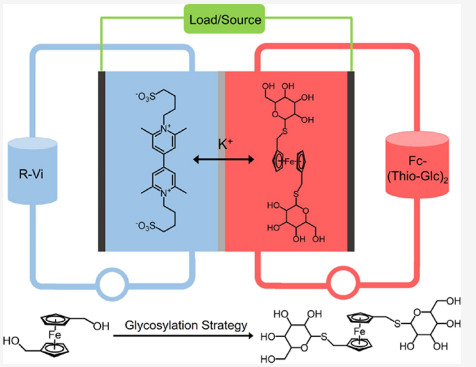

INTRODUCTION

Among existing electrochemical energy storage technologies, aqueous organic redox flow batteries (AORFBs) emerge as a particularly appealing option for their environmental friendliness and adaptability.[1−9] To enhance the energy density of AORFBs, numerous solubilization modification strategies for organic active molecules have been developed.[10−17] Nevertheless, the present synthetic approaches generally involve multistep reaction sequences and laborious postsynthetic purification processes, exhibiting limited structural diversification. Such limitations underscore the critical need to develop innovative solubilizing moieties with enhanced aqueous solubility and streamlined synthetic accessibility. Sugars, also referred to as carbohydrates, are omnipresent and indispensable nutrients in organisms. Carbohydrates are a renewable natural resource derived widely from grains, tubers, and fruits, allowing for a sustainable supply through cultivation and harvest. Furthermore, carbohydrates, particularly monosaccharides and disaccharides, possess exceptional hydrophilicity stemming from their polyhydroxyl structure. Notably, their solubilizing feature extends across diverse pH environments, making them an attractive candidate as a molecular functionalization reagent. However, to date, the exploitation of saccharide moieties as solubilizing auxiliaries has remained conspicuously absent from the extant literature.

Herein, we introduce a bioinspired glycosylation strategy utilizing thioetherification reactions to graft glucose onto redox-active molecules under mild conditions, yielding a highly soluble glycosyl ferrocene (Fc) derivative, 1,1′-bis(β-D-glucopyranosylthiomethyl)ferrocene (Fc(Thio-Glc)$_2$). The resulting Fc(Thio-Glc)$_2$ compound exhibited a redox potential of 0.28 V (vs Ag/AgCl) at neutral pH. Molecular dynamics (MD) simulations were conducted to elaborate a thorough analysis of the changes in the number of hydrogen bonds among components in the Fc(Thio-Glc)$_2$ system. The multitudinous highly polar hydroxyl moieties in Fc(Thio-Glc)$_2$ spontaneously form hydrogen bond networks with water molecules, and the cyclic architecture of monosaccharide side

Received: July 11, 2025
Revised: September 27, 2025
Accepted: September 30, 2025

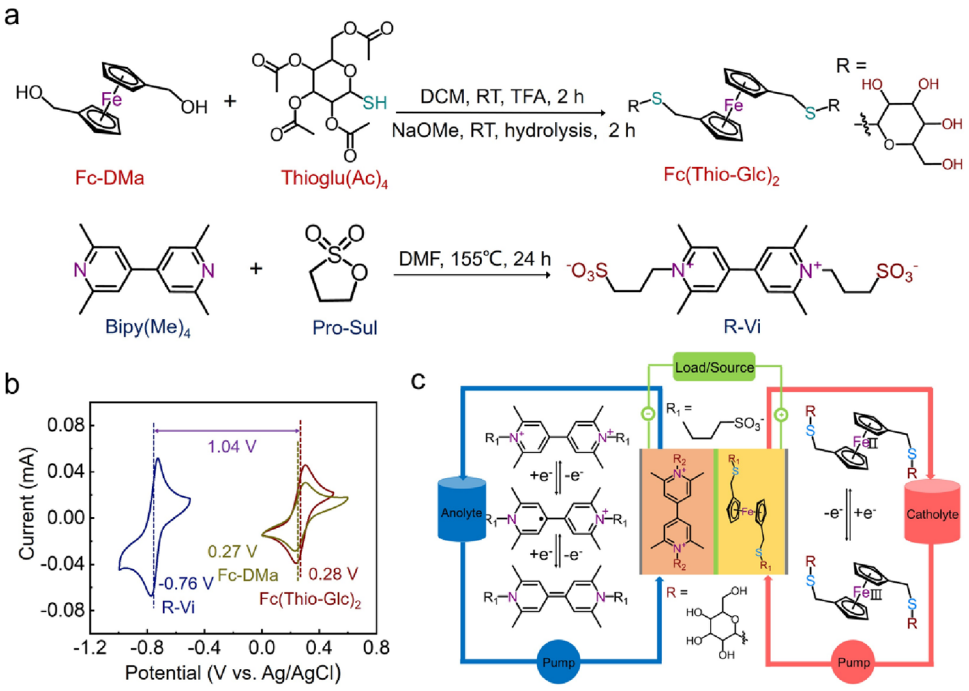

Figure 1. (a) Synthesis routes of $Fc(Thio\text{-}Glc)_2$ and R-Vi utilized in this work. (b) CV curves of 4.0 mM $Fc(Thio\text{-}Glc)_2$, R-Vi, and Fc-DMa in 1.0 M KCl solution at a scan rate of 100 mV s^{-1}. (c) Schematic diagram of the AORFBs based on the $Fc(Thio\text{-}Glc)_2$ catholyte and R-Vi anolyte.

groups maximizes the exposure of polar functionalities, creating all-around hydrophilic domains that facilitate the formation of stable hydration shells with water molecules. Therefore, $Fc(Thio\text{-}Glc)_2$ demonstrates high water solubility (1.3 M in 1.0 M KCl solution) and good electrochemical performances. Comprehensive spectroscopic analyses verified the excellent reversibility and stability of $Fc(Thio\text{-}Glc)_2$ during long-term cycling. When paired with a bis(3-sulfonatopropyl)-2,2′,6,6′-tetramethyl-4,4′-bipyridine (R-Vi) based anolyte, the as-fabricated AORFBs, with a 0.5 M $Fc(Thio\text{-}Glc)_2$ catholyte, exhibited a minimal capacity fade rate of 0.005% per cycle or 0.18% per day over 400 cycles. This study underscores the immense potential of bioinspired molecular engineering strategies in propelling the development of safe, stable, and sustainable ARFBs, paving the way for their application in large-scale energy storage systems.

RESULTS AND DISCUSSION

Fc derivatives have emerged as promising catholytes in AORFBs, demonstrating notable advantages including a well-suited redox potential, exceptional stability, and favorable molecular tunability through various chemical modifications.[18−23] Nevertheless, most existing functionalization methods are time-consuming and require complex synthesis steps with low yields. Natural carbohydrates are a class of highly water-soluble molecules with multiple hydrophilic hydroxyl groups. Inspired by natural sugar compounds, we designed a thioglucose functionalization strategy to synthesize highly soluble Fc derivatives via convenient thioetherification reactions under mild conditions. Figure 1a illustrates the synthesis routes of $Fc(Thio\text{-}Glc)_2$ and R-Vi to be employed as cathodic and anodic active molecules, respectively. The treatment of 1,1′-ferrocenedimethanol (Fc-DMa) and 2-(acetoxymethyl)-6-mercaptotetrahydro-2H-pyran-3,4,5-triyl triacetate ($Thioglu(Ac)_4$) with trifluoroacetic acid at room temperature for 2 h resulted in the grafting of two thiol-acetylglucose side groups. Subsequent deprotection of acetyl groups in NaOMe solution at room temperature for 2 h afforded the final product $Fc(Thio\text{-}Glc)_2$ with an overall yield of 88%. R-Vi was prepared via the *N*-alkylation reaction of 2,2′,6,6′-tetramethyl-4,4′-bipyridine ($Bipy(Me)_4$) and 1,3-propane sultone (Pro-Sul). In contrast to conventional synthesis routes, the synthesis approach proposed in this study stands out for its utilization of nature-inspired sugar precursors, low-boiling point organic solvents, short completion time, and mild reaction conditions, hence avoiding the subsequent complicated purification and impurity removal steps. The high purities of $Fc(Thio\text{-}Glc)_2$ and R-Vi final products were confirmed by ^1H and ^{13}C nuclear magnetic resonance (NMR) characterizations and high-resolution electrospray ionization mass spectrometry (HRESIMS), as shown in Figures S1−S6.

The redox potentials of $Fc(Thio\text{-}Glc)_2$ and R-Vi were measured to be 0.28 and −0.76 V (vs Ag/AgCl), respectively, leading to a theoretical cell voltage of 1.04 V (Figure 1b). The redox potential of Fc-DMa in 1.0 M KCl solution was 0.27 V (vs Ag/AgCl), which is slightly lower than that of $Fc(Thio\text{-}glc)_2$. The structural configuration of AORFBs based on the $Fc(Thio\text{-}Glc)_2$ catholyte and R-Vi anolyte is shown in Figure 1c. Based on UV−vis absorbance measurements, the maximum solubilities of $Fc(Thio\text{-}Glc)_2$ and Fc-DMa in 1.0 M KCl solutions were determined to be 1.3 and 0.035 M (Figure S7), respectively, indicating the effectiveness of the glycosylation strategy on water solubilization. The viscosity of $Fc(Thio\text{-}Glc)_2$ with different concentrations in water and 1.0 M KCl solution is shown in Figure S8. At concentrations of 0.5 and 1.3 M, the viscosity values of $Fc(Thio\text{-}Glc)_2$ were 1.35 and 1.85 mPa·s in 1.0 M KCl solution, respectively. The groundbreaking utilization of carbohydrates as solubilizing groups for organic active species in AORFBs opens up a realm that has thus far remained unreported.

https://doi.org/10.1021/jacs.5c11833
J. Am. Chem. Soc. XXXX, XXX, XXX−XXX

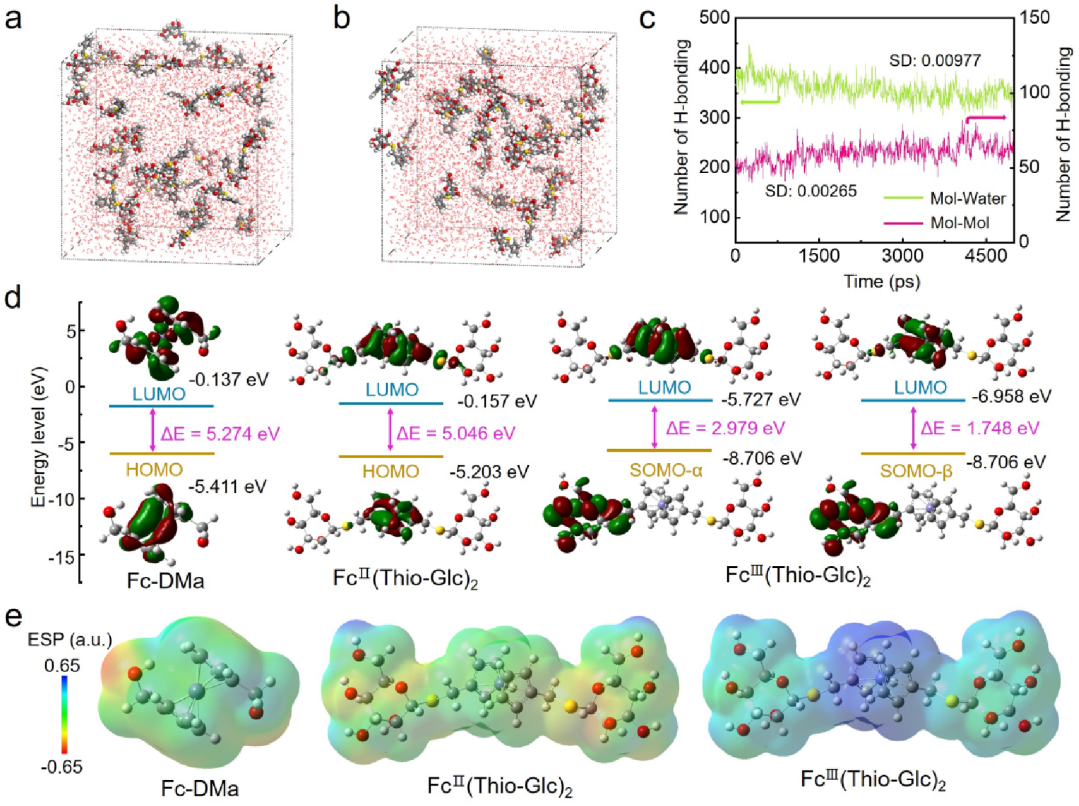

Figure 2. (a, b) Conformation diagrams for the MD simulation system of $Fc(Thio\text{-}Glc)_2$ molecules interacting with water molecules at initial and final states. (c) The number of hydrogen bonds over time for Mol-Water and Mol-Mol in the entire system (Mol represents $Fc(Thio\text{-}Glc)_2$). (d) Molecular orbitals and energy gaps of Fc-DMa, $Fc^{II}(Thio\text{-}Glc)_2$, and $Fc^{III}(Thio\text{-}Glc)_2$. (e) Optimized structures and electrostatic potentials of Fc-DMa, $Fc^{II}(Thio\text{-}Glc)_2$, and $Fc^{III}(Thio\text{-}Glc)_2$.

As reported in the prior literature, bipyridinium derivatives typically undergo two-electron reduction, manifesting two distinct redox peaks in CV curves. The experimental data for the R-Vi anolyte reveal that two redox peaks are indeed located at −0.76 and −1.08 V (vs Ag/AgCl) (Figure S9). However, the second reduction step of the R-Vi anolyte exhibits an irreversible behavior. To resolve this issue, we implemented a precise voltage control strategy during charge/discharge processes, ensuring that R-Vi participates exclusively in a single-electron redox reaction. In addition, the potential gap between $Fc(Thio\text{-}Glc)_2$ and R-Vi was theoretically predicted to be approximately 1.15 V by using the DFT methods, which matched well with the experimental value of 1.04 V (Table S1 and Figure 1b).

Molecular dynamics (MD) simulations provided crucial mechanistic insights into the hydrogen bonding networks in the entire system generated by $Fc(Thio\text{-}Glc)_2$.[24] The investigation revealed significant alterations in the quantity and nature of hydrogen bonds of $Fc(Thio\text{-}Glc)_2$ molecules that interacted with water molecules, as illustrated in Figure 2a,b. Specifically, Figure 2c reveals an augmentation in the number of hydrogen bonds within the Mol-Mol interactions (Mol represents $Fc(Thio\text{-}Glc)_2$), primarily OH···OH and S···OH bonds, whereas hydrogen bonds between $Fc(Thio\text{-}Glc)_2$ and water molecules (Mol-Water) decreased. The standard deviations of the hydrogen bond number for Mol-Mol and Mol-Water were 0.00265 and 0.00977, respectively. These findings indicate a pronounced aggregation between $Fc(Thio\text{-}Glc)_2$ molecules and a concurrent reduction in the interfacial contact area between $Fc(Thio\text{-}Glc)_2$ and water molecules. In addition, two unique bond angles were observed, one forming between $Fc(Thio\text{-}Glc)_2$ and water molecules and another within $Fc(Thio\text{-}Glc)_2$ molecules themselves (Figure S10a). According to Figure S10b, the $Fc(Thio\text{-}Glc)_2$ molecule was encapsulated within a solvated shell comprising multiple water molecules with an intermolecular distance of 1.78 Å. Within a single $Fc(Thio\text{-}Glc)_2$ molecule, the intermolecular distance between the two glucose chains was approximately 1.62 Å. Conversely, the distance between glucose chains belonging to two distinct $Fc(Thio\text{-}Glc)_2$ molecules was approximately 2.62 Å. These findings highlight the structural stability and solubility contributions of hydrogen bonding networks within the $Fc(Thio\text{-}Glc)_2$ based aqueous electrolyte.

Figure 2d shows a comparison of the highest occupied molecular orbital (HOMO) and lowest unoccupied molecular orbital (LUMO) energy levels for Fc-DMa, $Fc^{II}(Thio\text{-}Glc)_2$, and $Fc^{III}(Thio\text{-}Glc)_2$. The results revealed that $Fc^{II}(Thio\text{-}Glc)_2$ possesses a narrower energy gap than that of Fc-DMa after grafting two carbohydrate side groups. When losing one electron, $Fc^{III}(Thio\text{-}Glc)_2$ exhibited the smallest energy gap between the LUMO and SOMO-α/SOMO-β level. Generally, a lower LUMO energy level of organic species indicates a higher potential for reduction.[25,26] The LUMO energy level of $Fc^{II}(Thio\text{-}Glc)_2$ (−0.137 eV) was slightly lower than that of Fc-DMa (−0.157 eV), indicating a higher potential of $Fc^{II}(Thio\text{-}Glc)_2$ (0.28 V) than Fc-DMa (0.27 V). These calculation results are in accordance with the CV results in Figure 1b. DFT simulations were further carried out to obtain the optimized structures and electrostatic potential (ESP) levels for Fc-DMa, $Fc^{II}(Thio\text{-}Glc)_2$, and $Fc^{III}(Thio\text{-}Glc)_2$

https://doi.org/10.1021/jacs.5c11833
J. Am. Chem. Soc. XXXX, XXX, XXX−XXX

molecules. As illustrated in Figure 2e, Fc(Thio-Glc)$_2$ exhibited a more negative ESP compared to Fc-DMa, which is attributed to the incorporation of highly polar hydroxyl groups. The grafted carbohydrate side groups boost polarizability, thereby encouraging hydration and the formation of hydrogen bonds. This interplay enhances the spacing between water molecules and in turn facilitates the dissolution of Fc(Thio-Glc)$_2$.

The redox reaction kinetics of Fc(Thio-Glc)$_2$ were investigated by linear sweep voltammetry (LSV), as shown in Figures S11. All three experiments were conducted in 1.0 M KCl solution with a 1.0 mM concentration of the active species. The diffusion coefficient (D) was obtained from the Levich plot of the limiting diffusion currents and the square roots of the rotation rates (Levich equation). As the rotation rates increased from 200 to 2000 rpm at a scan rate of 25 mV s^{-1} (Figure S11a–c), the D value of Fc(Thio-Glc)$_2$ was calculated to be 4.43 × 10^{-6} cm^2 s^{-1} based on three tests (Figure S11d–f). By fitting the Butler–Volmer equation to Levich plots (Tafel equation) (Figure S11g–i), the electron-transfer rate constant (k_0) was calculated to be 5.30 × 10^{-3} cm s^{-1} based on three tests (Figure S11j–l). The corresponding standard deviations for D and k_0 were 0.18 and 0.04, respectively. (Figure S11m–n). The D and k_0 values of Fc(Thio-Glc)$_2$ exhibited a similar order of magnitude among other catholyte species.[15−20,15−20,27−30] As the scan rate increased from 25 to 5000 mV s^{-1}, both the oxidation and reduction peak currents had a linear relationship with the square root of the scan rate ($\nu^{1/2}$), indicating a reversible and diffusion-controlled redox process (Figure S12a).[31−33] The slope ratios of cathodic and anodic scans were calculated to be close to 1, indicating that the oxidized and reduced Fc(Thio-Glc)$_2$ molecules had similar diffusion coefficients (Figure S12b). Moreover, the CV curves of Fc(Thio-Glc)$_2$ exhibited a complete overlap and revealed no additional peaks after 50 cycles (Figure S12c), demonstrating its remarkable electrochemical reversibility with the absence of side reactions.

The working performances of AORFBs coupled by the Fc(Thio-Glc)$_2$ catholyte and excess R-Vi anolyte at a low concentration of 0.1 M are shown in Figure 3. The electrolytes consisted of 5.0 mL of 0.1 M Fc(Thio-Glc)$_2$ catholyte and 7.5 mL of 0.2 M R-Vi anolyte in 1.0 M KCl solutions. A pretreated Nafion-212 membrane was employed as the separator between catholyte and anolyte. Electrochemical impedance spectroscopy (EIS) analysis revealed that the impedance of the Nafion separator in 1.0 M KCl solution was 0.57 Ω cm^2 (Figure S13a), while the permeability of Fc(Thio-Glc)$_2$ solution through this separator was as low as 5.38 × 10^{-10} cm^2 s^{-1} (Figure S13b). We also conducted an extra permeation experiment based on 0.5 M Fc(Thio-Glc)$_2$ and 0.5 M R-Vi in 1.0 M KCl solutions. The UV–vis crossover curve of the R-Vi solution was displayed to confirm the permeation change when the two solutions were stored together for 10 days (Figure S14). However, the absorption peaks of Fc(Thio-Glc)$_2$ and R-Vi at $\lambda_{210\ nm}$ and $\lambda_{206\ nm}$, as well as at $\lambda_{252\ nm}$ and $\lambda_{260\ nm}$, are very close. Due to the overlap of the absorption peaks, it was difficult to determine the exact permeability of Fc(Thio-Glc)$_2$ in this experiment. The R-VII|Fc(Thio-Glc)$_2$ AORFB demonstrated an open-circuit voltage (OCV) exceeding 1.0 V, aligned with the above CV measurements. At 20 and 50 mA cm^{-2}, the AORFB delivered discharge capacities of 2.5 and 2.3 Ah L^{-1}, respectively (Figure 3a,b). Upon galvanostatic cycling at 40 mA cm^{-2} between 1.2 and 0.6 V, the R-VII|Fc(Thio-Glc)$_2$ AORFB exhibited a discharge capacity of 2.4 Ah L^{-1} during the

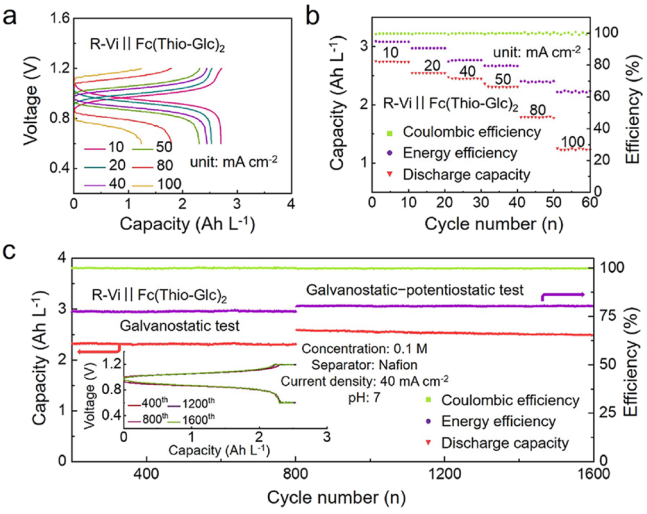

Figure 3. Working performances of Fc(Thio-Glc)$_2$ based AORFBs at a low concentration. The catholyte was 5.0 mL of 0.1 M Fc(Thio-Glc)$_2$ in 1.0 M KCl solution, and the anolyte was 7.5 mL of 0.2 M R-Vi in 1.0 M KCl solution. (a) Typical galvanostatic charge/discharge curves of R-VII|Fc(Thio-Glc)$_2$ AORFB at various current densities of 10, 20, 40, 50, 80, and 100 mA cm^{-2} between 1.2 and 0.6 V. (b) Discharge capacities, Coulombic efficiencies, and energy efficiencies of R-VII|Fc(Thio-Glc)$_2$ AORFB at different current densities. (c) Long-term cycling performances of the R-VII|Fc(Thio-Glc)$_2$ AORFB under galvanostatic mode for the initial 800 cycles and then galvanostatic-potentiostatic mode for the later 800 cycles.

initial 800 cycles with no apparent capacity decay, which is 90.0% of its theoretical capacity (2.68 Ah L^{-1}) (Figure 3c). The Coulombic efficiencies remained consistently close to 100%, and the energy efficiencies reached above 75% during the cycling processes. Subsequently, galvanostatic-potentiostatic cycling was also performed upon the same battery for the later 800 cycles. The AORFB was charged to 1.2 V at a current density of 40 mA cm^{-2} with the potential holding at 1.2 V until the current density dropped to 5 mA cm^{-2} and then was discharged to 0.6 V at a current density of 40 mA cm^{-2} with the potential holding at 0.6 V until the current density dropped to 5 mA cm^{-2}. As the cycling continued, the charge/discharge plateaus remained unaltered, and the battery exhibited a low capacity fade rate of 0.0023% cycle^{-1} for the subsequent 800 cycles. Figure S15a shows the OCVs of R-VII|Fc(Thio-Glc)$_2$ AORFB at different states of charge (SOCs). The OCVs at 50% SOC were measured to be 1.0 V for Fc(Thio-Glc)$_2$ and reached 1.12 V at 100% SOC. The polarization curves of R-VII|Fc(Thio-Glc)$_2$ AORFBs were measured by LSV at different concentrations (Figure S15b). The power densities of R-VII|Fc(Thio-Glc)$_2$ AORFBs with 0.2 and 0.5 M Fc(Thio-Glc)$_2$ catholytes reached 70 and 90 mW cm^{-2} at 100% SOC, respectively.

The long-term cycling test of R-VII|Fc(Thio-Glc)$_2$ AORFBs with 0.5 and 0.2 M Fc(Thio-Glc)$_2$ catholyte is shown in Figure 4a and Figure S16. The catholyte was 5.0 mL of 0.2 or 0.5 M Fc(Thio-Glc)$_2$ in 1.0 M KCl solution, and the anolyte was 7.5 mL of 0.4 or 1.0 M R-Vi in 1.0 M KCl solution. At a current density of 40 mA cm^{-2} between 1.2 and 0.6 V, the R-VII|Fc(Thio-Glc)$_2$ AORFB based on 0.2 M Fc(Thio-Glc)$_2$ delivered a discharge capacity of 4.95 Ah L^{-1} (i.e., 92.3% utilization of theoretical capacity, 5.36 Ah L^{-1}) and maintained a low capacity fade rate of 0.004% cycle^{-1} after 700 cycles. At different current densities of 20, 40, 50, 60, 80, and 100 mA

https://doi.org/10.1021/jacs.5c11833
J. Am. Chem. Soc. XXXX, XXX, XXX–XXX

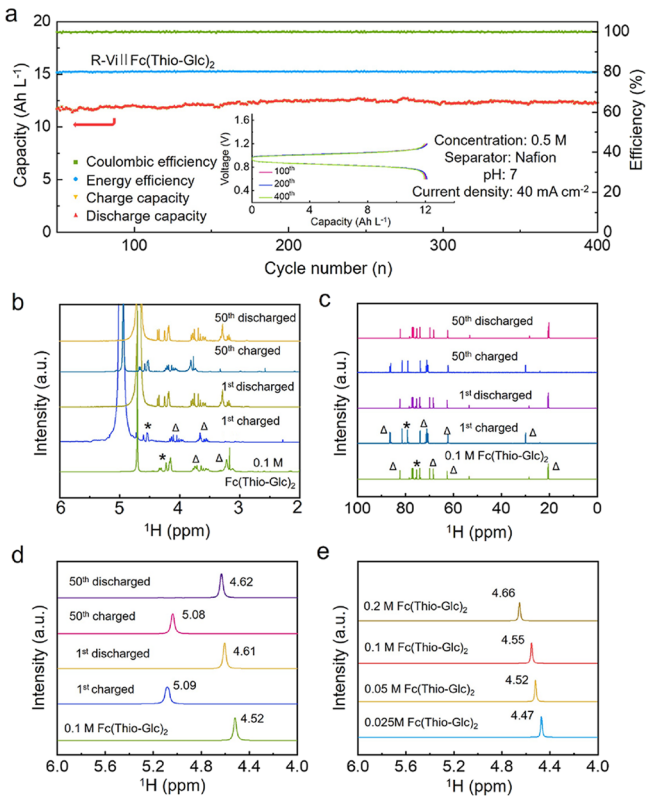

Figure 4. Electrochemical behaviors of the Fc(Thio-Glc)$_2$ catholyte. (a) Galvanostatic cycling performances of R-Vi||Fc(Thio-Glc)$_2$ AORFBs with 0.5 M Fc(Thio-Glc)$_2$ catholyte operated at 40 mA cm^{-2} between 1.2 and 0.6 V. The inset shows the charge/discharge curves at different cycles. (b, c) No-D ^{1}H NMR and ^{13}C NMR spectra of the Fc(Thio-Glc)$_2$ catholyte after fully charged and discharged in the 1st and the 50th cycles, respectively. The peaks in the cyclopentene unit of Fc(Thio-Glc)$_2$ are marked with "*" (Fc-H), and those in the glucose unit of Fc(Thio-Glc)$_2$ are marked with "Δ" (GL-H). (d) The water peak regions magnified from the dashed box in (b). (e) No-D ^{1}H NMR spectra of the water peaks in Fc(Thio-Glc)$_2$ catholytes with various concentrations (0.025−0.2 M).

cm^{-2}, the discharge capacities of the R-Vi||Fc(Thio-Glc)$_2$ AORFB based on 0.5 M Fc(Thio-Glc)$_2$ were 13.2, 12.1, 11.9, 11.6, 10.3, and 8.4 Ah L^{-1}, and the corresponding energy efficiency values were 89.8%, 81.5%, 80.4%, 78.8%, 70.3%, and 65.8%, respectively (Figure S17). Upon galvanostatic cycling at 40 mA cm^{-2}, the R-Vi||Fc(Thio-Glc)$_2$ AORFB based on the 0.5 M Fc(Thio-Glc)$_2$ catholyte delivered a discharge capacity of 11.92 Ah L^{-1} (i.e., 89.0% of theoretical capacity, 13.4 Ah L^{-1}) with a capacity fade rate of 0.005% cycle^{-1} (i.e., 0.18% day^{-1}) after 400 cycles (i.e., 12.1 days). During the entire cycling process, the Coulombic efficiency maintained a near-perfect 100%, while the energy efficiency surpassed 70%. The comprehensive electrochemical performance of R-Vi||Fc(Thio-Glc)$_2$ AORFB was compared with those of other Fc derivative based AORFB systems (Tables S2 and S3).[15−20,15−20,28−30] Although the synthesis cost of Fc(Thio-Glc)$_2$ is slightly elevated, experimental validation demonstrated that the Fc derivative functionalized with carbohydrates exhibit a highly improved aqueous solubility. This study represents a pioneering exploration of carbohydrate-based solubilizing groups in AORFBs. In theory, the water solubility of carbohydrates demonstrates remarkable pH robustness, functioning effectively across acidic, neutral, and alkaline conditions simultaneously. In view of the efficient synthesis, obvious aqueous solubility enhancement of Fc(Thio-Glc)$_2$, and sustainable characteristics of nature-inspired carbohydrates, subsequent research could employ alternative synthetic strategies to integrate carbohydrate moieties with more cost-effective redox-active molecules such as anthraquinone or phenazine derivatives, thereby expanding the applicability of this approach.

To further elucidate the electrochemical behaviors of the Fc(Thio-Glc)$_2$ catholyte, No-D ^{1}H and ^{13}C NMR analyses were employed to monitor the structural stability of Fc(Thio-Glc)$_2$ during cycling.[34,35] Unlike conventional NMR, No-D NMR spectra are unaffected by deuterated solvents, allowing them to accurately reflect the intrinsic signals of Fc(Thio-Glc)$_2$ accurately. To ensure a fully charged state, the battery was charged to 1.2 V and maintained at that potential for 5 min. Upon charging, the signals of protons in cyclopentene ("*", Fc-H) and glucose ring (Δ, GL-H) broadened and shifted toward higher chemical shifts; upon discharging, these peaks sharpened and reverted toward their initial positions (Figure 4b). For example, the Fc-H peaks at 4.0 and 4.4 ppm shifted to 4.5 and 4.9 ppm ($\Delta\delta$ = 0.4 ppm) after charging to 1.2 V and restored to 4.0 and 4.4 ppm ($\Delta\delta$ = −0.4 ppm) after discharging to 0.6 V. In the No-D ^{13}C NMR spectra (Figure 4c), the carbon peaks of Fc(Thio-Glc)$_2$ almost have a similar variation trend upon charge/discharge processes. Water solvent resonance shifts mirrored these trends, reflecting the changes in the magnetic susceptibility of the electrolyte (Figure 4d). After 50 galvanostatic cycles, the proton peaks of water shifted back to their initial positions, confirming the high redox reversibility of Fc(Thio-Glc)$_2$. Furthermore, the No-D ^{1}H NMR spectra of Fc(Thio-Glc)$_2$ catholytes with different concentrations (0.025−0.2 M) were also analyzed (Figure 4e). The chemical shifts of water proton peaks can reflect the quantity of hydrogen bonds in the Fc(Thio-Glc)$_2$ system. When the concentration increased from 0.025 to 0.2 M, the water proton peaks apparently shifted downfield from 4.47 to 4.66 ppm, which is attributed to the increase of hydrogen bond formation. The above No-D ^{1}H NMR data reveal the hydrogen bond interactions between Fc(Thio-Glc)$_2$ with water molecules, further confirming the formation of hydrogen bond networks in the Fc(Thio-Glc)$_2$ catholyte system.

To elucidate the structural stability and potential performance attenuation mechanism of Fc(Thio-Glc)$_2$ during cycling, we analyzed the ^{1}H NMR spectra of the Fc(Thio-Glc)$_2$ catholyte and R-Vi anolyte stored at high temperature or after 400 galvanostatic cycles. The R-Vi anolyte and Fc(Thio-Glc)$_2$ catholyte were left to stand at 60 °C for 20 days and characterized by ^{1}H NMR spectroscopy (Figure S18). The elevated temperature stability test of them revealed unchanged spectra, indicating their stable molecular structures at high temperatures.[36−38] For the Fc(Thio-Glc)$_2$ catholyte after long-term cycling, some newly proton peaks emerged at 3.0−4.5 ppm (marked as "*"), suggesting a small portion of solubilizing group detachment from the Fc core and the dimers of cyclopentadiene (Figure 5a and Figure S19a). According to previous studies, Fc derivatives may react with water to form new coordination complexes, whereas two cyclopentadienyl ligands spontaneously assemble into irreversible dimers (Figure S19b).[20] This degradation mechanism involves a nucleophilic attack on the Fc metallic center, initiating dissociation via ligand exchange, reduction by cyclopentadiene ions, and dimerization or polymerization of cyclopentadienyl

https://doi.org/10.1021/jacs.5c11833
J. Am. Chem. Soc. XXXX, XXX, XXX−XXX

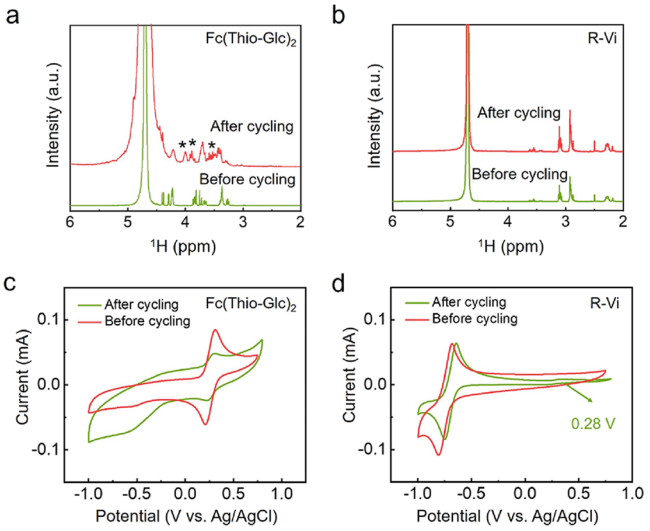

Figure 5. Long-term stability mechanism studies of high-concentration Fc(Thio-Glc)$_2$ based AORFBs. (a, b) Ex situ ^{1}H NMR spectra of the Fc(Thio-Glc)$_2$ catholyte and R-Vi anolyte before and after 400 galvanostatic cycles, respectively. The peaks marked with "*" represent the degraded impurities in the Fc(Thio-Glc)$_2$ catholyte. (c, d) CV curves of the Fc(Thio-Glc)$_2$ catholyte and R-Vi anolyte before and after 400 galvanostatic cycles, respectively.

radicals. The HRESIMS analysis also confirmed the formation of a trace amount of single-side functionalized Fc-Thio-Glc byproduct and dimerization radicals (Figure S20). These results indicated that the observed degradation of Fc derivatives is electrochemically induced. Meanwhile, the ^{1}H NMR spectra of the R-Vi anolyte remained almost unchanged (Figure 5b). Postcycle CV curves of the Fc(Thio-Glc)$_2$ catholyte and R-Vi anolyte after cycling were also collected (Figure 5c). Conversely, a prominent oxidation/reduction peak at 0.28 V emerged in the CV curve of the R-Vi anolyte after cycling (Figure 5d), corroborating the slight crossover of Fc(Thio-Glc)$_2$ molecules during cycling.[39] These results indicate that no discernible impurity that affects the battery performance appeared from the R-Vi anolyte. Although the side-chain hydrolysis and dimerization increase during cycling, it has a tiny influence on the integrity of the Fc core, and the abundant hydrogen bond interactions of glucose groups immobilize more water molecules within the solvation shell of Fc(Thio-Glc)$_2$, effectively suppressing the degradation of the Fc core. Consequently, Fc(Thio-Glc)$_2$ exhibits better stability compared to most existing Fc derivatives.

CONCLUSIONS

In summary, this study introduced a glycosylation-based solubilization strategy, culminating in the creation of a polyhydric glycosyl ferrocene derivative, Fc(Thio-Glc)$_2$, via a convenient thioetherification reaction. The incorporation of multiple hydrophilic hydroxyl groups bestowed Fc(Thio-Glc)$_2$ with an unprecedented aqueous solubility of 1.3 M in 1.0 M KCl solution. MD simulations verified the formation and favorable effects of hydrogen bond networks between Fc(Thio-Glc)$_2$ and water molecules on the molecular configuration and solvation behavior. The pH-neutral AORFBs based on a high-concentration Fc(Thio-Glc)$_2$ catholyte achieved exceptional capacity retention and cycling stability, corresponding to a lower capacity fade rate of 0.005% per cycle or 0.18% per day over 400 cycles. A series of spectroscopic analyses elucidated the redox reversibility and long-term stability mechanisms of the Fc(Thio-Glc)$_2$ catholyte and R-Vi anolyte. This pioneering glycosylation modification exemplifies the vast potential of leveraging nature-inspired molecular designs to enhance the solubility and functionality of redox-active organic species. By bridging the principles of green chemistry with advanced energy storage systems, this work paves the way to develop high-performance AORFBs and reimagines the role of natural derivatives in sustainable energy solutions.

ASSOCIATED CONTENT

Supporting Information

The Supporting Information is available free of charge at https://pubs.acs.org/doi/10.1021/jacs.5c11833.

Experimental section and additional figures and tables, including NMR spectra, HRESIMS spectra, CV curves, EIS curves, electrochemical measurements, and battery performance tests; Figures S1−S20 and Table S1−S3 (PDF)

AUTHOR INFORMATION

Corresponding Authors

Zuoxiu Tie − *State Key Laboratory of Coordination Chemistry, MOE Key Laboratory of Mesoscopic Chemistry, MOE Key Laboratory of High Performance Polymer Materials and Technology, Jiangsu Key Laboratory of Advanced Organic Materials, Suzhou Key Laboratory of Green Intelligent Manufacturing of New Energy Materials and Devices, Tianchang New Materials and Energy Technologies Research Center, Institute of Green Chemistry and Engineering, School of Chemistry and Chemical Engineering, Nanjing University, Nanjing, Jiangsu 210023, P. R. China*; Email: zxtie@nju.edu.cn

Yichao Yan − *State Key Laboratory of Coordination Chemistry, MOE Key Laboratory of Mesoscopic Chemistry, MOE Key Laboratory of High Performance Polymer Materials and Technology, Jiangsu Key Laboratory of Advanced Organic Materials, Suzhou Key Laboratory of Green Intelligent Manufacturing of New Energy Materials and Devices, Tianchang New Materials and Energy Technologies Research Center, Institute of Green Chemistry and Engineering, School of Chemistry and Chemical Engineering, Nanjing University, Nanjing, Jiangsu 210023, P. R. China*; Email: ychyan@nju.edu.cn

Zhong Jin − *State Key Laboratory of Coordination Chemistry, MOE Key Laboratory of Mesoscopic Chemistry, MOE Key Laboratory of High Performance Polymer Materials and Technology, Jiangsu Key Laboratory of Advanced Organic Materials, Suzhou Key Laboratory of Green Intelligent Manufacturing of New Energy Materials and Devices, Tianchang New Materials and Energy Technologies Research Center, Institute of Green Chemistry and Engineering, School of Chemistry and Chemical Engineering, Nanjing University, Nanjing, Jiangsu 210023, P. R. China*; orcid.org/0000-0001-8860-8579; Email: zhongjin@nju.edu.cn

Authors

Guochun Ding − *State Key Laboratory of Coordination Chemistry, MOE Key Laboratory of Mesoscopic Chemistry, MOE Key Laboratory of High Performance Polymer Materials and Technology, Jiangsu Key Laboratory of Advanced Organic Materials, Suzhou Key Laboratory of*

https://doi.org/10.1021/jacs.5c11833
J. Am. Chem. Soc. XXXX, XXX, XXX−XXX

Green Intelligent Manufacturing of New Energy Materials and Devices, Tianchang New Materials and Energy Technologies Research Center, Institute of Green Chemistry and Engineering, School of Chemistry and Chemical Engineering, Nanjing University, Nanjing, Jiangsu 210023, P. R. China

Tianyu Shen − *State Key Laboratory of Coordination Chemistry, MOE Key Laboratory of Mesoscopic Chemistry, MOE Key Laboratory of High Performance Polymer Materials and Technology, Jiangsu Key Laboratory of Advanced Organic Materials, Suzhou Key Laboratory of Green Intelligent Manufacturing of New Energy Materials and Devices, Tianchang New Materials and Energy Technologies Research Center, Institute of Green Chemistry and Engineering, School of Chemistry and Chemical Engineering, Nanjing University, Nanjing, Jiangsu 210023, P. R. China*

Pengbo Zhang − *State Key Laboratory of Coordination Chemistry, MOE Key Laboratory of Mesoscopic Chemistry, MOE Key Laboratory of High Performance Polymer Materials and Technology, Jiangsu Key Laboratory of Advanced Organic Materials, Suzhou Key Laboratory of Green Intelligent Manufacturing of New Energy Materials and Devices, Tianchang New Materials and Energy Technologies Research Center, Institute of Green Chemistry and Engineering, School of Chemistry and Chemical Engineering, Nanjing University, Nanjing, Jiangsu 210023, P. R. China*

Zuoao Wu − *State Key Laboratory of Coordination Chemistry, MOE Key Laboratory of Mesoscopic Chemistry, MOE Key Laboratory of High Performance Polymer Materials and Technology, Jiangsu Key Laboratory of Advanced Organic Materials, Suzhou Key Laboratory of Green Intelligent Manufacturing of New Energy Materials and Devices, Tianchang New Materials and Energy Technologies Research Center, Institute of Green Chemistry and Engineering, School of Chemistry and Chemical Engineering, Nanjing University, Nanjing, Jiangsu 210023, P. R. China*

Qianchuan Yu − *State Key Laboratory of Coordination Chemistry, MOE Key Laboratory of Mesoscopic Chemistry, MOE Key Laboratory of High Performance Polymer Materials and Technology, Jiangsu Key Laboratory of Advanced Organic Materials, Suzhou Key Laboratory of Green Intelligent Manufacturing of New Energy Materials and Devices, Tianchang New Materials and Energy Technologies Research Center, Institute of Green Chemistry and Engineering, School of Chemistry and Chemical Engineering, Nanjing University, Nanjing, Jiangsu 210023, P. R. China*

Yuzhu Liu − *State Key Laboratory of Coordination Chemistry, MOE Key Laboratory of Mesoscopic Chemistry, MOE Key Laboratory of High Performance Polymer Materials and Technology, Jiangsu Key Laboratory of Advanced Organic Materials, Suzhou Key Laboratory of Green Intelligent Manufacturing of New Energy Materials and Devices, Tianchang New Materials and Energy Technologies Research Center, Institute of Green Chemistry and Engineering, School of Chemistry and Chemical Engineering, Nanjing University, Nanjing, Jiangsu 210023, P. R. China*

Sheng Wen − *State Key Laboratory of Coordination Chemistry, MOE Key Laboratory of Mesoscopic Chemistry, MOE Key Laboratory of High Performance Polymer Materials and Technology, Jiangsu Key Laboratory of Advanced Organic Materials, Suzhou Key Laboratory of Green Intelligent Manufacturing of New Energy Materials and Devices, Tianchang New Materials and Energy Technologies Research Center, Institute of Green Chemistry and Engineering, School of Chemistry and Chemical Engineering, Nanjing University, Nanjing, Jiangsu 210023, P. R. China*

Jie Wei − *Energy & Environmental Materials Research Department, Suzhou Laboratory, Suzhou, Jiangsu 215125, P. R. China*

Complete contact information is available at: https://pubs.acs.org/10.1021/jacs.5c11833

Notes

The authors declare no competing financial interest.

■ ACKNOWLEDGMENTS

The authors appreciate the financial support from the National Natural Science Foundation of China (22479074, 22475096), the Equipment Pre-Research and Ministry of Education Joint Fund (8091B02052407), the Fundamental Research Program Key Project of Jiangsu Province (BK20253008), the Natural Science Foundation of Jiangsu Province (BK20240400, BK20241236), the Science and Technology Major Project of Jiangsu Province (BG2024013), the Scientific and Technological Achievements Transformation Special Fund of Jiangsu Province (BA2023037), the Academic Degree and Postgraduate Education Reforming Project of Jiangsu Province (JGKT24_C001), the Key Core Technology Open Competition Project of Suzhou City (SYG2024122), the Open Research Fund of Suzhou Laboratory (SZLAB-1308-2024-TS005), and the Chenzhou National Sustainable Development Agenda Innovation Demonstration Zone Provincial Special Project (No. 2023sfq11).

■ REFERENCES

(1) Xia, M.; Fu, H.; Li, K.; Rao, A.; Cha, L.; Liu, H.; Zhou, J.; Wang, C.; Liu, B. Hydrogen-Bond Regulation in Organic/Aqueous Hybrid Electrolyte for Safe and High-Voltage K-Ion Batteries. *Energy Environ. Sci.* **2024**, *17* (3), 1255−1265.

(2) Fu, J.; Xu, J.; Zhang, Y.; Zhang, L.; Lan, X.; Feng, Y.; Gong, W.; Guo, J.; Yong, Z.; Li, Q. Metal-Organic Framework-Derived NiS_2 Nanoflowers Supported on Carbon Nanotube Fibers for Aqueous Rechargeable Nikel-Zinc Batteries. *ACS Appl. Nano Mater.* **2024**, *7* (2), 2214−2223.

(3) Deng, S.; Meng, W.; Fan, C.; Zuo, D.; Han, J.; Li, T.; Li, D.; Jiang, L. Enabling Further Organic Electrolyte Infiltration of Cellulose-Based Separators via Defect-Rich Polypyrrole Modification for High Sodium Ion Transport in Sodium Metal Batteries. *ACS Appl. Mater. Interfaces* **2024**, *16* (4), 4708−4718.

(4) Choi, Jy.; Park, Jo.; Park, Ji.; Kim, Ms.; Lee, So.; Cho, Ch.; Lee, Ji.; Park, Yi.; Kim, Gy.; Choi, Ja.; Park, Ju.; Park, Mj. Low-Index Facet Polyhedron-Shaped Binary Ccerium Titanium Oxide for High-Voltage Aqueous Zinc-Vanadium Redox Flow Batteries. *ACS Appl. Mater. Interfaces* **2023**, *15* (48), 55692−55702.

(5) Murata, T.; Hamasaki, M.; Morita, Y. A Benzoquinone-Imidazole Hybrid Organic Anolyte for Aqueous Redox Flow Batteries. *Chem. Commun.* **2024**, *60* (7), 878−880.

(6) Feng, R.; Chen, Y.; Zhang, X.; Rousseau, B.; Gao, P.; Chen, P.; Mergelsberg, S.; Zhong, L.; Hollas, A.; Liang, Y.; Murugesan, V.; Huang, Q.; Walter, E.; Hammes-Schiffer, S.; Shao, Y.; Wang, W. Proton-Regulated Alcohol Oxidation for High-Capacity Ketone-Based Flow Battery Anolyte. *Joule* **2023**, *7* (7), 1609−1622.

(7) Liu, Y.; Zhang, P.; Wu, Z.; Wei, J.; Ding, G.; Song, X.; Ma, J.; Wang, W.; Jin, Z. Screening Ultra-Stable (Phenazine)Dioxyalkanocic

Acids with Varied Water-Solubilizing Chain Lengths for High-Capacity Aqueous Redox Flow Batteries. *J. Am. Chem. Soc.* **2024**, *146* (5), 3293−3302.
(8) Schwan, S.; Schröder, D.; Wegner, H.; Janek, J.; Mollenhauer, D. Substituent Pattern Effects on the Redox Potentials of Quinone-Based Active Materials for Aqueous Redox Flow Batteries. *ChemSusChem* **2020**, *13* (20), 5480−5488.
(9) Feng, R.; Zhang, X.; Murugesan, V.; Hollas, A.; Chen, Y.; Shao, Y.; Walter, E.; Wellala, N.; Yan, L.; Rosso, M.; Wang, W. Reversible Ketone Hydrogenation and Dehydrogenation for Aqueous Organic Redox Flow Batteries. *Science* **2021**, *372* (6544), 836−840.
(10) Wu, M.; Bahari, M.; Fell, E.; Gordon, R.; Aziz, J. High-Performance Anthraquinone with Potentially Low Cost for Aqueous Redox Flow Batteries. *J. Mater. Chem. A* **2021**, *9* (47), 26709−26716.
(11) Pang, S.; Jin, S.; Yang, F.; Alberts, M.; Li, L.; Xi, D.; Gordon, R.; Wang, P.; Aziz, M.; Ji, Y. A Phenazine-Based High Capacity and High-Stability Electrochemical CO_2 Capture Cell with Coupled Electricity Storage. *Nat. Energy* **2023**, *8*, 1126−1136.
(12) Yao, Y.; Ma, W.; Lei, J.; Wang, Z.; Lu, Y.; Liu, L. Nonionic Oligo(Ethylene Glycol)-Substituted Viologen Negolytes for Aqueous Organic Redox Flow Batteries. *J. Mater. Chem. A* **2023**, *11* (24), 12984−12991.
(13) Ambrose, B.; Naresh, R.; Deshmukh, S.; Kathiresan, M.; Ragupathy, P. Exploring Contemporary Advancements and Outlook in Viologen-Based Aqueous Organic Redox Flow Batteries: A Mini Review. *Energy Fuel* **2023**, *37* (23), 18226−18242.
(14) Pan, M.; Gao, L.; Liang, J.; Zhang, P.; Lu, S.; Lu, Y.; Ma, J.; Jin, Z. Reversible Redox Chemistry in Pyrrolidinium-Based TEMPO Radical and Extended Viologen for High-Voltage and Long-Life Aqueous Redox Flow Batteries. *Adv. Energy Mater.* **2022**, *12* (13), No. 2103478.
(15) Zhao, Z.; Zhang, B.; Schrage, B.; Ziegler, C.; Boika, A. Investigations into Aqueous Redox Flow Batteries Based on Ferrocene Bisulfonate. *ACS Appl. Energy Mater.* **2020**, *3* (10), 10270−10277.
(16) Kim, S.; Kim, D.; Hwang, G.; Jeon, J. A Bromide-Ligand Ferrocene Derivative Redox Species with High Reversibility and Electrochemical Stability for Aqueous Redox Flow Batteries. *Electroanalytical Chem.* **2020**, *869*, No. 114131.
(17) Beh, E. S.; De Porcellinis, D.; Gracia, R. L.; Xia, K. T.; Gordon, R. G.; Aziz, M. J. A Neutral pH Aqueous Organic-Organometallic Redox Flow Battery with Extremely High Capacity Retention. *ACS Energy Lett.* **2017**, *2*, 639−644.
(18) Hu, B.; DeBruler, C.; Rhodes, Z.; Liu, L. Long-Cycling Aqueous Organic Redox Flow Battery (AORFB) toward Sustainable and Safe Energy Storage. *J. Am. Chem. Soc.* **2017**, *139* (3), 1207−1214.
(19) Chen, Q.; Li, Y.; Liu, Y.; Sun, P.; Yang, Z.; Xu, T. Designer Ferrocene Catholyte for Aqueous Organic Flow Batteries. *ChemSusChem* **2021**, *14* (5), 1295−1301.
(20) Li, Y.; Xu, Z.; Liu, Y.; Jin, S.; Fell, E.; Wang, B.; Gordon, R.; Aziz, M.; Yang, Z.; Xu, T. Functioning Water-Insoluble Ferrocenes for Aqueous Organic Flow Battery via Host-Guest Inclusion. *ChemSusChem* **2021**, *14* (2), 745−752.
(21) Liu, B.; Li, Y.; Jia, G.; Zhao, T. Recent Advanced in Redox Flow Batteries Employing Metal Coordination Complexes as Redox-Active Species. *Electrochem. Energy Rev.* **2024**, *7* (1), 7−36.
(22) Kim, S.; Yoon, T.; Kim, Y.; Hwang, S.; Ryu, J.; Oh, S. Increase of Both Solubility and Working Voltage by Acetyl Substitution on Ferrocene for Non-Aqueous Flow Battery. *Electrochem. Commun.* **2016**, *69*, 72−75.
(23) Song, H.; Kwon, G.; Citek, C.; Jeon, S.; Kang, K.; Lee, E. Pyrrolinium-Substituted Persistent Zwitterionic Ferrocenate Derivative Enabling the Application of Ferrocene Anolyte. *ACS Appl. Mater. Interfaces* **2021**, *13* (39), 46558−46565.
(24) Peng, C.; Ning, G. H.; Su, J.; Zhong, G.; Tang, W.; Tian, B.; Su, C.; Yu, D.; Zu, L.; Yang, J.; Ng, M. F.; Hu, Y. S.; Yang, Y.; Armand, M.; Loh, K. P. Reversible Multi-Electron Redox Chemistry of p-Conjugated N-Containing Heteroaromatic Molecule Based Organic Cathodes. *Nat. Energy* **2017**, *2*, 17074.
(25) Tie, Z.; Zhang, Y.; Zhu, J.; Bi, S.; Niu, Z. An Air Rechargeable Zn/Organic Battery with Proton Storage. *J. Am. Chem. Soc.* **2022**, *144* (23), 10301−10308.
(26) Liu, X.; Zhang, H.; Liu, C.; Wang, Z.; Zhang, X.; Yu, H.; Zhao, Y.; Li, M.; Li, Y.; He, Y.; He, G. Commercializable Naphthalene Diimide Anolytes for Neutral Aqueous Organic Redox Flow Batteries. *Angew. Chem. Int. Ed.* **2024**, *63* (25), No. e202405247.
(27) Pang, S.; Wang, X.; Wang, P.; Ji, Y. Biomimetic Amino Acid Functionalized Phenazine Flow Batteries with Long Lifetime at Near-Neutral pH. *Angew. Chem. Inter. Ed.* **2021**, *60* (10), 5289−5298.
(28) Yao, Y.; Xu, H.; Tian, Z.; Zhang, J.; Zhan, F.; Yan, M.; Jia, C. Simple-Synthesized Sulfonated Ferrocene Ammonium for Aqueous Redox Flow Batteries. *ACS Appl. Energy Mater.* **2021**, *4* (8), 8052−8058.
(29) Luo, J.; Hu, B.; Debruler, C.; Bi, Y.; Zhao, Y.; Yuan, B.; Hu, M.; Wu, W.; Liu, T. Unprecedented Capacity and Stability of Ammonium Ferrocyanide Catholyte in pH Neutral Aqueous Redox Flow Batteries. *Joule* **2019**, *3* (1), 149−163.
(30) Li, X.; Gao, P.; Lai, Y. Y.; Bazak, J. D.; Hollas, A.; Lin, H. Y.; Murugesan, V.; Zhang, S.; Cheng, C. F.; Tung, W. Y.; Lai, Y. T.; Feng, R.; Wang, J.; Wang, C. L.; Wang, W.; Zhu, Y. Symmetry-Breaking Design of an Organic Iron Complex Catholyte for a Long Cyclability Aqueous Organic Redox Flow Battery. *Nat. Energy* **2021**, *6* (9), 873−881.
(31) Luo, J.; Sam, A.; Hu, B.; Debruler, C.; Wei, X.; Wang, W.; Liu, L. Unraveling pH Dependent Cycling Stability of Ferricyanide/Ferrocyanide in Redox Flow Batteries. *Nano Energy* **2017**, *42*, 215−221.
(32) Chen, Q.; Lv, Y.; Yuan, Z.; Li, X.; Yu, G.; Yang, Z.; Xu, T. Organic Electrolytes for pH-Neutral Aqueous Organic Redox Flow Batteries. *Adv. Funct. Mater.* **2021**, *32* (9), No. 2108777.
(33) Luo, J.; Hu, B.; Hu, M.; Zhao, Y.; Liu, T. Status and Prospects of Organic Redox Flow Batteries toward Sustainable Energy Storage. *ACS Energy Lett.* **2019**, *4* (9), 2220−2240.
(34) Pan, M.; Cao, N.; Lin, W.; Luo, X.; Chen, K.; Che, S.; Li, H.; Wang, C. Reversible CO_2 Capture by Conjugated Ionic Liquids Through Dynamic Covalent Carbon-Oxygen Bonds. *ChemSusChem* **2016**, *9* (17), 2351−2357.
(35) Zhao, E.; Liu, T.; Jonsson, E.; Lee, J.; Temprano, I.; Jethwa, R.; Wang, A.; Smith, H.; Carretero-Gonzalez, J.; Song, Q.; Grey, C. In Situ NMR Metrology Reveals Reaction Mechanisms in Redox Flow Batteries. *Nature* **2020**, *579* (7798), 224−228.
(36) Xu, J.; Pang, S.; Wang, X.; Wang, P.; Ji, Y. Ultrastable Aqueous Phenazine Flow Batteries with High Capacity Operated at Elevated Temperatures. *Joule* **2021**, *5* (9), 2437−2449.
(37) Kwabi, D. G.; Lin, K.; Ji, Y.; Kerr, E. F.; Goulet, M. A.; De Porcellinis, D.; Tabor, D. P.; Pollack, D. A.; Aspuru-Guzik, A.; Gordon, R. G.; Aziz, M. J. Alkaline Quinone Flow Battery with Long Lifetime at pH 12. *Joule* **2018**, *2* (9), 1894−1906.
(38) Ji, Y.; Goulet, M.; Pollack, D. A.; Kwabi, D. G.; Jin, S.; De Porcellinis, D.; Kerr, E. F.; Gordon, R. G.; Aziz, M. J. A Phosphonate-Functionalized Quinone Redox Flow Battery at Near-Neutral pH with Record Capacity Retention rate. *Adv. Energy Mater.* **2019**, *9* (12), No. 1900039.
(39) Chai, J.; Wang, X.; Lashgari, A.; Williams, C.; Jiang, J. A pH-Neutral Aqueous Redox Flow Battery with a 3600-cycle Lifetime: Micellization-Enabled High Stability and Crossover Suppression. *ChemSusChem* **2020**, *13* (16), 4069−4077.

https://doi.org/10.1021/jacs.5c11833
J. Am. Chem. Soc. XXXX, XXX, XXX−XXX